SAND2016-2652C

A MONTE CARLO PERCOLATION METHOD APPLIED TO THE DECOMPOSITION OF AMMONIUM PERCHLORATE

W. W. Erikson
Sandia National Laboratories*
Albuquerque, NM

ABSTRACT

One of the most intriguing aspects of ammonium perchlorate (AP) decomposition is its incomplete decomposition at low temperatures, in which the decomposition halts at a level of approximately 30%. Various theories have been proposed to explain this observation based on physical and chemical arguments. Here we consider the notion that geometry itself might contribute to this limiting value. Percolation theory involves the "connectedness" of a geometric lattice, and a network is said to percolate if it is connected continuously end-to-end. It has been demonstrated that in a cubic lattice, percolation occurs at a site density of ~31.1%, remarkably similar to the limiting void fraction in AP. A Monte Carlo (MC) algorithm using simple rules has been developed and applied to particle decomposition. The MC simulations result in porosity evolutions that are reminiscent of actual AP behavior in terms of the overall limiting porosity which is developed, the effect of particle size, and the sigmoidal time response.

INTRODUCTION

***Ammonium Perchlorate*.**

The thermal decomposition of ammonium perchlorate (NH_4ClO_4, a.k.a. AP) has been investigated for many decades. It may be one of the most well-studied energetic materials in history [1]. Yet its decomposition behavior is not yet completely understood. There are two basic processes by which AP breaks down, and these processes generally occur in tandem. First is the dissociative sublimation process whereby AP changes into gas phase NH_3 and $HClO_4$. This is a "surface" phenomenon—sublimation rates are proportional to the particle surface area and sublimation can be suppressed by increasing the surrounding gas pressure. The second process is the temperature-driven decomposition / breakdown of AP into product species, and is the one principally dealt with here. Our purpose is not to fully describe the various AP decomposition data and theories, but rather to examine one particular aspect—the peculiar cessation that occurs with low temperature decomposition.

At high temperatures (>300°C), AP particles will decom-pose to completion; its final products are all gas phase molecules. At low temperatures (<300°C) the sublimation is slow and decomposition has been observed to cease, often at about 30% mass loss [2], particularly for AP powders consisting of large particles. Testing with smaller sizes has resulted in lower mass losses (see Fig. 1), to wit: 34-35% for 250-355 μm diameter particles, 25-33% for nominal 200 μm, 29% for 75-106 μm, 23% for 50 μm, 20% for 20-38 μm, 11% for "crushed" (~10 μm) and interestingly at 3-4 μm particle

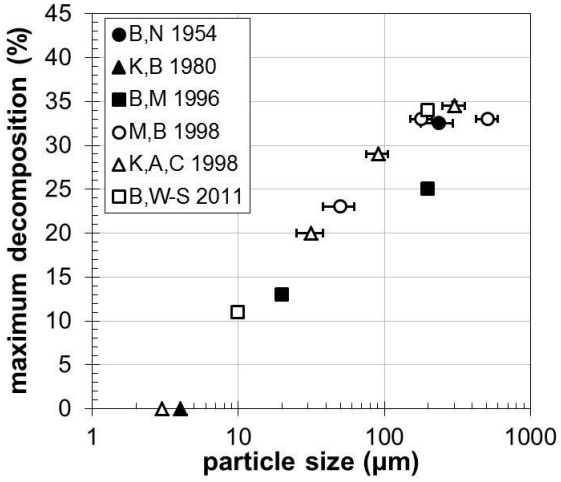

Fig. 1: Total decomposition mass loss as a function of particle size (Refs. [2-8]). Bars represent range of sizes in bin.

Statement A: Approved for public release; distribution is unlimited.

* Sandia National Laboratories is a multi-program laboratory managed and operated by Sandia Corporation, a wholly owned subsidiary of Lockheed Martin Corporation, for the U.S. Department of Energy's National Nuclear Security Administration under contract DE-AC04-94AL85000. This work was performed with funding from the DoD/DOE Joint Munitions Program TCG-III.

size, no decomposition (sublimation still occurs) [2, 3, 4, 5, 6, 7, 8]. Chemical analysis shows that the residual solid is pure AP [1, 2].

AP has two polymorphs—an orthorhombic crystal phase below ~240°C and a cubic phase above that temperature. Figure 2 shows a diagram of the orthorhombic state and illustrates the various crystal faces and their characteristics [9, 10]. The lattice cell includes 4 molecules and has dimensions of a=9.20, b=5.82, c=7.45 Å implying a density of ρ=1.95 g/cm^3. The cubic phase has a unit cell length of a=7.63 Å with a density of 1.76 g/cm^3. The low temperature cessation is *not* associated with the material phase—it has been observed in both orthorhombic and cubic phase AP. The enhanced reactivity that occurs with some materials due to increased ion lattice mobility during a phase change (Hedvall effect) does not appear to occur with AP. On the contrary, there is a *drop* in reaction rate as AP changes phase: "the rate of thermal decomposition sharply decreases at the moment of phase transition" [11], although the cause of this "reverse Hedvall effect" [11] is not clear, it could be because reaction nuclei have been altered by the phase change, or perhaps due to a drop in material density (lattice spacing increases) or a catalytic effect which occurs at a higher rate for the orthorhombic form [8].

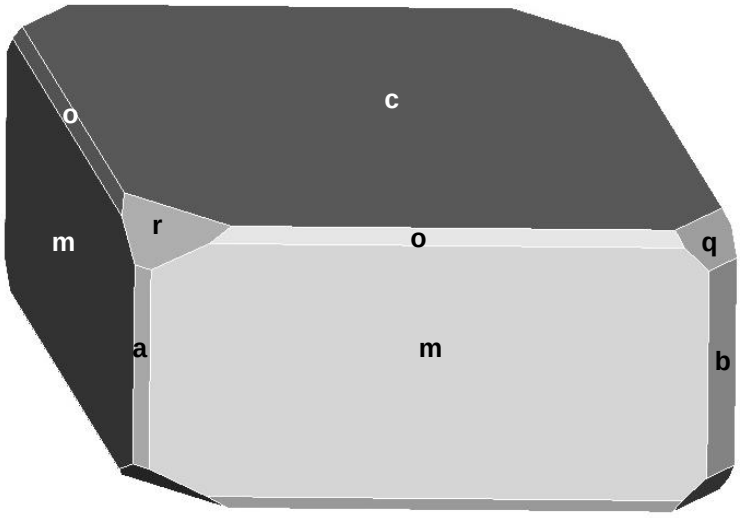

Miller Indices	
a:	100
b:	010
c:	001
m:	210
o:	211
q:	011
r:	101

Unit Cell (n=4)
a=9.20 Å
b=5.82 Å
c=7.45 Å
cubic:
a=7.63 Å

Selected Angles			
ab:	90°00'	rc:	38°55'
ac:	90°00'	rr:	102°10'
bc:	90°00'	bq:	37°59'
aq:	90°00'	qc:	52°01'
br:	90°00'	ao:	45°11'
cm:	90°00'	oq:	44°49'
am:	38°25'	bo:	56°01'
mb:	51°35'	or:	33°59'
mm*:	76°50'	co:	64°07'
mm†:	103°10'	om:	25°53'
ar:	51°05'	mr:	60°31'

* around face a
† around face b

Fig. 2: Orthorhombic form of AP crystal with unit cell lengths from Boldyrev [11] and Miller indices and angles from Tutton [9]; some earlier references had incorrectly listed m face as index 110, which has occasionally been propagated through the literature as noted in Ref. [10]. According to Tutton, faces a, b, q, and o are often very small or not present, while faces c, m, and r are typically well-developed. Thus, the m face is often nearly perfectly rectangular while the c face is a rhombus.

There have been a number of theories put forward as to why the decomposition halts. It is notable that most of these theories are proposed by individuals that have considerable reputation and experience in the field of solid-state chemistry and thermal decomposition of solid materials. Their publication lists over the past several decades runs into the hundreds, and the theories themselves have been published in peer-reviewed archival journals of high standing. It is therefore unwise to summarily discount any of these hypotheses. Here we will attempt to describe each theory in unbiased terms. With this perspective, they are not arranged in any particular order. These mechanisms may operate in different regions of phase space and/or in tandem.

A. Differential Knudsen diffusion in pores.

This theory was developed by Boldyrev and associates several decades ago [12] and has been reaffirmed in a more recent document [11]. The process is described with two major steps. (1) First a proton transfers within the ionically bonded NH_4ClO_4 molecule resulting in formation of ammonia (NH_3) and perchloric acid ($HClO_4$) gases. These gases collect inside pores within the crystal. (2) Unequal rates

of Knudsen diffusion within pores (where the smaller NH_3 molecules can preferentially escape in contrast to the larger $HClO_4$ molecules which collide with the pore walls), results in a net accumulation of $HClO_4$ within the pores. The $HClO_4$ then decomposes and its reaction products react with the NH_4ClO_4 on the pore walls; this action increases the size of the pore. Eventually the pore size become large enough that the preferential Knudsen diffusion is eliminated and the $HClO_4$ no longer accumulates in the pores—effectively halting the decomposition process. This process does imply that the pores themselves are open-ended to permit the escape of the ammonia; the requisite separation of the two gases wouldn't be expected to occur in blind pores.

B. Pressure / Lattice Strain Effects

In contrast to the previous theory, the idea here is that decomposition reactions occur inside the crystal within blind pores below the surface of the particle. The decomposition reactions are initiated at crystal defects (pores, inclusions, etc.) within the crystal. The reactions are also presumed to be pressure-dependent. And since within the blind pores, material changes from solid to gas at near constant volume, the resulting gas pressure can become very high (some measurements have inferred gas pressures of 2 MPa within pore spaces [13], though this is likely low if the gases form at the original solid density). The high pressures induce stresses on the surrounding crystal lattice, resulting in localized lattice strain and the development of additional lattice defects which act as sites for reactions to occur. However, once the expanding pores have reached the particle surface, the gases vent, dropping the pressure and the reactions stop within that pore. Eventually possible reaction sites are depleted and the overall reaction ceases. The end result is a highly porous structure. This concept has been described by Behrens, Kay, and co-workers at Sandia, as well as Kraeutle at China Lake, and Raevskii in the former Soviet Union (see References [4, 5, 7, 14, 15]). Descriptive words such as "blisters" which "tended to break open" [14] and "spallation fragments" [15] are used to indicate that "subsurface reactions are responsible for the decomposition" [14].

C. *"Wormholing" by a Fluid/Liquid Reactive Intermediate*.

This theory was proposed by Galwey and Mohamed in the mid-1980s [1, 16]. The theory says that there is a reactive intermediate, namely liquid nitronium perchlorate (NO_2ClO_4, a.k.a. nitryl perchlorate, melting point 135°C) that is formed in some small quantity from AP decomposition. That liquid then catalyzes decomposition reactions of the AP at the bottom of ca. 0.2-0.5 μm diameter pores, producing final products. The nitronium perchlorate largely remains intact and continues to catalyze reaction at the bottom of the pore. It eats its way through the particle in a pseudo random fashion consuming AP in its path and leaving behind a "labyrinthine network of interconnected channels" [1] and larger (~5 μm) holes where individual channels combine. The decomposition of NO_2ClO_4 yields products which oxidize ammonia (or NH_4^+ ions) from the AP forming NO_2^+ ions which react with ClO_4 (also from AP) to re-form NO_2ClO_4 and maintain the catalyst's presence in the pore. Eventually the catalyst itself disappears (if the NO_2ClO_4 decomposes completely prior to reacting with additional AP) and at that point, the reaction rates essentially cease. The authors assert that cessation of reaction at ~70% mass remaining is probably due to the removal of the more reactive, imperfect surface regions which are susceptible to nucleation. Evidence supporting this theory includes these observations: (a) contact with various nitrate compounds significantly increases the decomposition rate of AP, (b) trace amounts of oxidized nitrogen compounds including NO_2ClO_4 have been detected in partially decomposed AP, (c) the activation energy for AP decomposition is similar to that reported for NO_2ClO_4 decomposition, and (d) the smoothly, rounded internal surfaces of the pores that formed by decomposition are indicative of liquid participation [16]. A key concept of this theory is that the reactions begin at the surface of the particle, not in the interior.

D. Nucleation Site Depletion

The basic idea is that the decomposition of ammonium perchlorate must begin at an appropriate nucleation site within the crystal lattice. These preferred nucleation sites might be dislocations, crystal defects, voids, or impurities, which disrupt the regularity of the crystal lattice. These nuclei grow as reactions progress. Decomposition would stop when (a) the existing nuclei stop growing (for whatever reason) and (b) no sites for additional nuclei formation are available. Some quotations from literature (mainly Khairetdinov and Boldyrev) relating to this are:

". . .nucleus formation takes place under the surface of the AP crystal. The germ formed first grows up to 2 μm and then stops" [8]

"[Chlorine] oxides may initiate the formation of a new germ 3-5 μm from the old one. The new germ cannot arise at a shorter distance for the same reasons as an old germ ceases to grow, i.e. due to H_2O accumulation" [8] (note: The authors of ref. [1] dispute that water is the cessation-inducing quantity, based on experiments in which the material was continually dried.)

"If the nucleation takes place on the AP surface it will cease immediately since the catalysts of LTD [low temperature decomposition]—intermediate products of $HClO_4$ decomposition—will escape out of the crystal" [8]

"highly dispersed specimens of AP (d < 4 μm) are stable under LTD conditions since the nucleation process can only take place on no less than 3-4 μm depth of an AP crystal" [8]

"The nucleation process *cannot* take place *deep* in the volume of the AP crystal due to the cell effect, i.e. steric difficulties . . . It is on the *subsurface* where the nucleation process proceeds most readily" [8], (emphasis added).

"the nuclei of the decompositional reaction do not have a legible boundary, and consist of a large number of spherical seeds (Ø 1-2μm). The formation and growth of the nuclei occur by means of a fusion of the seeds which originate close to the growing nucleus. . . . after generation, the seeds are in continuous motion until they fuse with the basic core of the nucleus" [15]

The above theories, while not completely agreeing in every aspect as to the fundamental explanations ("the why?"), yet provide some consistency into the observed behaviors. Nucleation, and the subsequent growth of those nuclei seem to be essential elements of the decomposition process. Nucleation must originate at or near the particle surface, preferentially at lattice defects. Growth of nuclei occurs for a time, but then self-limits due to physical or chemical effects (e.g. pressure venting or loss of reaction catalysts or accumulation of inhibiting products). Additional nuclei tend to form near existing reaction nuclei, possibly owing to reaction-induced lattice strain effects. The void space produced in partially decomposed AP is largely connected porosity.

Our goal here is to reproduce, (quantitatively, if possible) the low temperature decomposition behavior observed in ammonium perchlorate particles using numerical simulation. One aspect to be used is percolation theory. It is hoped that this will give additional insight into the decomposition behavior and promote additional thoughts, experiments, and models that may improve our understanding and ability to predict AP's behavior.

***Percolation Theory*.**

Percolation theory deals with the "connectedness" of an array of objects such as the molecules in a crystal lattice or the wires in a window screen. There are various forms of percolation. In describing them, two important concepts are defined: "sites" and "bonds." A "site" is a location of an object, a "bond" is the path or connection between two sites. The number of nearest neighboring sites that are connected to a given site is referred to as the "coordination number." A standard window screen is an example of a square lattice where the "sites" would be the intersections where the vertical and horizontal wires meet; it would have a coordination number of 4 with connections in the up, down, left, and right directions. "Percolation" itself refers to the situation when sites or bonds are fully connected from one end of the domain to another.

A bond percolation situation might deal with the bonds or connections such as the grid of wires in a window screen, whereas site percolation might deal with a regular stack of balls or blocks. Hunt [17] gives a couple of relevant examples that one might ask in describing percolation. For instance, a bond

percolation problem might be: if the wires in a window screen are cut one at a time, what fraction of them would need to remain so that the screen does not fall apart? (It turns out to be 50%.) Similarly, a site percolation problem might be: if a box is filled with balls (i.e. sites) of two types, plastic and metal, what fraction of the balls have to be metal so that the two ends of the box would have a continuous electrical pathway from one end of the box to the other? And because it depends on the number of continuous pathways, the electrical conductivity will be a function of the fraction of metal balls within the box. Percolation theory can represent this type of behavior.

The critical percolation limit (p_c) is the fraction of sites or bonds which just allows connection from one end to the other. In the window screen example above (2-D square lattice, bond percolation) p_c is exactly 0.5. For many lattices, an analytic formula for p_c is not available; it must be estimated numerically. Hunt [17] tabulates critical percolation values for various lattices; some of his values are reproduced here in Table I. In the table, graphical representations of the various lattices are given with dots representing the sites and lines representing the bonds (note: for the BCC lattice, the unit cells are plotted using dotted lines, with the 8 bonds as solid lines; for FCC, the unit cells are plotted, but for clarity, the bonds between the central site and the 12 neighboring sites are not shown, instead the central and neighboring sites are shown as solid dots). The coordination number, Z, represents the number of nearest neighboring sites to a given site. A similar number of nearest neighboring *bonds* to a given *bond* is listed as Z_{bond}. The critical percolation limits for site percolation and bond percolation are given. Note that the p_c values for bond percolation are generally lower than for site percolation; this phenomena is related to the number of nearest neighbors being higher for bonds than for sites.

Table I: Critical percolation thresholds for selected 2-D and 3-D lattices. Adapted from Hunt [17].

Lattice Type	Honeycomb	Square	Triangular	Diamond	Simple Cubic	BCC	FCC
Graphic	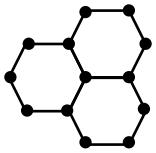	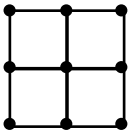	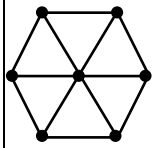	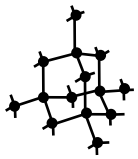	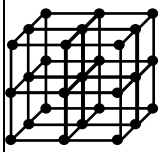	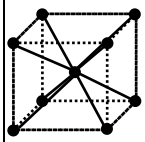	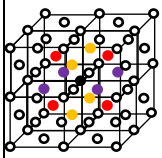
Coordination Number, Z	3	4	6	4	6	8	12
p_c (site)	0.6962	0.5927	0.5	0.4299	**0.3116**	0.2464	0.199
Z_{bond}	4	6	10	6	10	14	22
p_c (bond)	1-2sin(π/18) = 0.6527	0.5	2sin(π/18) = 0.3473	0.3886	0.2488	0.1795	0.119

Of particular interest for this work (and highlighted in the table), is the critical site percolation threshold for a simple cubic lattice (with six neighbors: up, down, left, right, front, back) which has an empirically determined value of 0.3116, or about 31%. This says, in essence, that for a structure consisting of stacked blocks, if blocks are randomly removed one at a time (each leaving a hole) then once about 31% of the blocks have been replaced by void space, there will be a continuous path of void space from one end of the structure to the other. This 31% level is reminiscent of the limiting void fraction resulting from the low temperature decomposition of ammonium perchlorate.

Our hypothesis is that the continuous network of voids produced in decomposed AP is a percolating network and that we can use percolation theory to examine its behavior. Of the seven lattice structures listed in Table I, we believe that the simple cubic structure most closely resembles AP. The low temperature orthorhombic structure can be considered a “stretched” cubic lattice with neighbors in the up, down, left, right, front and back directions. Naturally the high temperature cubic polymorph also fits this geometry. Our goal here is to develop a percolation theory-based Monte Carlo representation of decomposition to discover whether the notion is sound.

MODEL

A Monte Carlo (MC) algorithm was developed to test the hypothesis formulated above. In so doing we have liberally applied concepts from the very efficient Newman-Ziff algorithm [18]. But instead of simply assigning a spatially randomized once-and-for all insertion order for decomposition order as a the original Newman-Ziff MC approach might employ, we have used a somewhat more complex set of rules which are designed to mimic some of the observed behavior from AP decomposition as described in the introduction. Here we list the steps or rules that were applied.

Monte Carlo Algorithm Rules

1. A 2-D or 3-D domain is chosen; we allow rectangles or ellipses in 2-D and parallelepipeds or ellipsoids (including spheres) in 3-D. The domain is divided into uniform boxes (squares in 2-D, cubes in 3-D). The domain is initially all filled. Locations within the domain are chosen at random to "decompose" (change from solid to gas, forming a void).
2. A "zone of reactivity" near the outer edge of the domain is the only place where reactions can initially occur.
3. Insertion of a void induces a "stress" or "defect" in surrounding material, which extends the zone of reactivity around the void location (in all our examples, the zone of reactivity will extended by 2 boxes in every direction from an inserted void).
4. Voids cannot be inserted adjacent to the outer surface or adjacent to voids that are connected to the outer surface UNLESS they are also adjacent to another, unconnected (blind) void. This is to mimic the observed phenomena that decomposition begins at the subsurface (near the surface, but not on the surface), and that the gas pressure within a blind void can push its way out.
5. "Adjacent" for purposed of connecting voids is only at the box faces (baseline 2-D has 4 neighbors: left, right, up, down; baseline 3-D has 6 neighbors: left, right, up, down, front, back). Boxes that are touching only at corners are assumed to not be connected in the baseline configuration, though this assumption will be relaxed later on.
6. The algorithm stops when no more voids can be inserted and all voids are connected to the outside. Statistics such as void fraction as a function of number of MC steps are reported.

Two simple examples of the above algorithm are shown in Figs. 3 and 4. Each of these has a 12x12 square array that is initially filled. The zone of reactivity is defined (indicated by squares with a "+") initially in the first two interior layers; the surface layer is not included. Voids are placed at random locations within the zone of reactivity. Blind (unconnected to outside) are shown as squares with an "O" and voids connected to the exterior as empty squares. Disallowed (unreactive) regions are indicated by solid gray (far in the interior, away from any void sites) or "X" (adjacent to either the outside or to voids connected to the outside but at the same time NOT adjacent to an unconnected, blind void). As the voids are placed, the zone of reactivity is altered to mimic the condition where preferential nucleation sites exist near existing nucleated sites by replacing the deep interior material (gray goes away). Eventually as voids continue to be inserted, the algorithm reaches a state where the zone of reactivity itself goes away (no potential nucleation sites exist) leaving only non-reactive material and porosity which is connected with the exterior.

Figure 3 gives the baseline results—the case where the neighbors of a site for connection purposes are only those sharing the four faces (left, right, up, down). In this example, the algorithm completes when 64 of the 144 sites are converted to void (44% porosity). We expect that the results for a small, coarse problem such as this 12x12 example to be highly variable; if several runs were made, results would likely vary significantly. A larger domain should give a more consistent set of results. It should also be pointed out that while there are similarities, the algorithm we have implemented here is not exactly the same algorithm for which the site percolation limits were derived in Table I (e.g. 0.5927 void fraction for site percolation on the square lattice). We have included various limiters to mimic the behavior of the AP crystal decomposition. In addition, our algorithm does not guarantee that voids are completely connected end-to-end, just that every void is connected to the outside somewhere, and that no additional voids can be inserted.

Figure 4 shows a repeat of the algorithm but this time with the definition of "neighbor" adjusted such that the stencil includes the corners as well as the left-right-up-down faces so there are 8 neighbors instead of 4. In this instance, because the inclusion of diagonal neighbors, it is easier for pores to become connected to the outside. The result of this is that the total porosity at completion is lower. In the example, 43 of the 144 sites are converted to void, representing ~30% porosity. This second case is to illustrate the effect of including more neighbors.

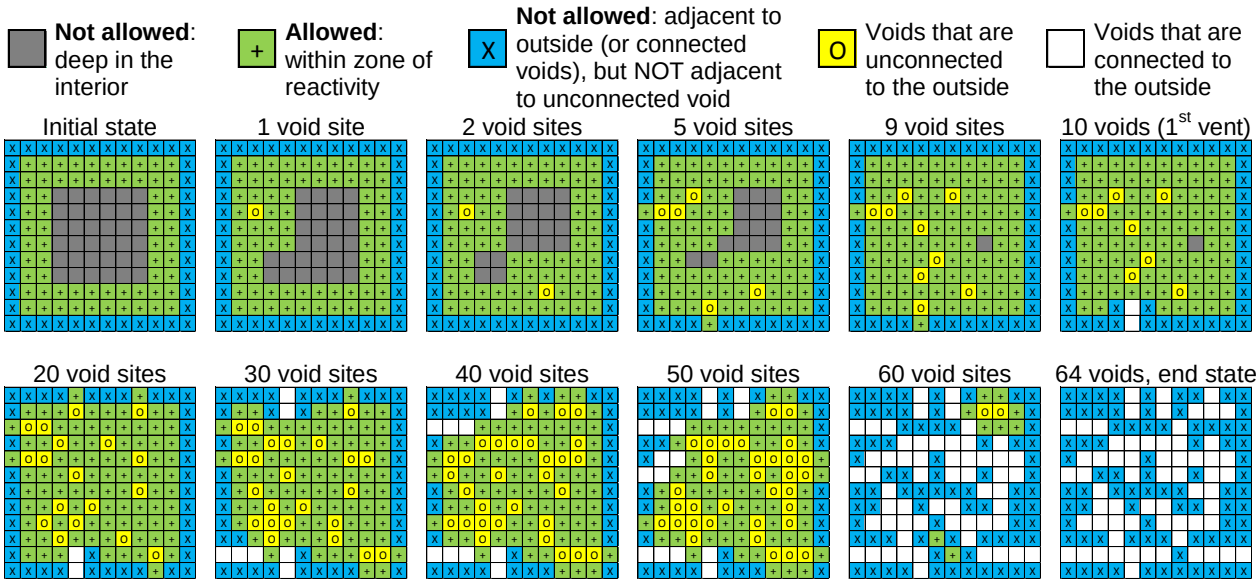

Fig. 3: Example of algorithm application on a 2-D 12x12 grid. 4 neighbors are included in stencil (faces at up, down, left, right). In this case, the algorithm terminates at 64/144 voids (44%).

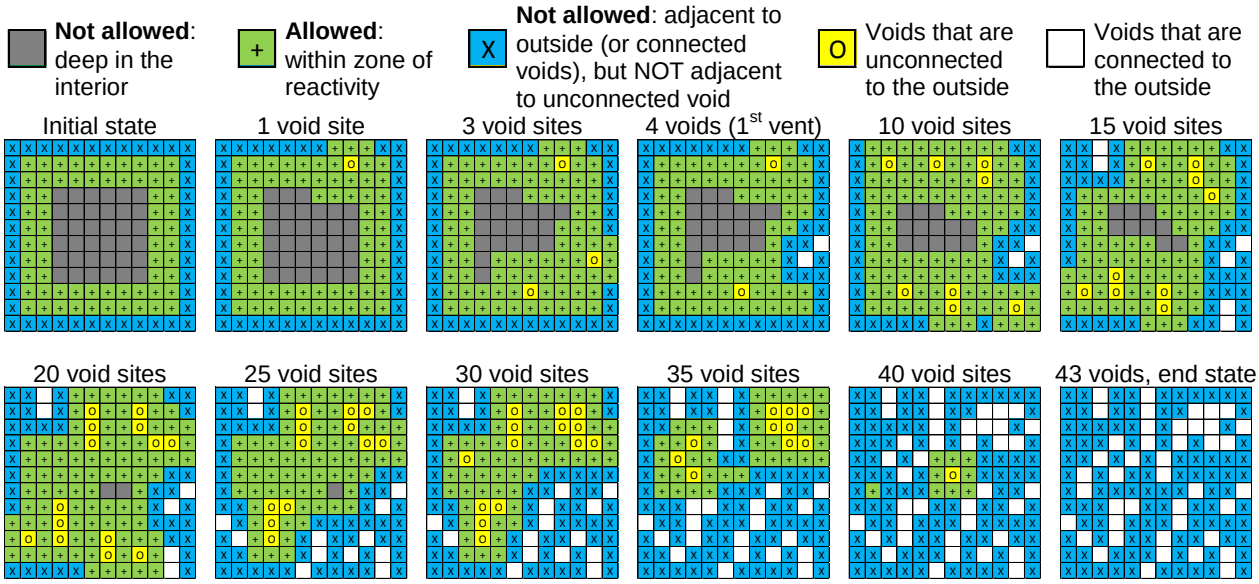

Fig. 4: Example of algorithm application on a 2-D 12x12 grid. 8 neighbors are included in stencil (faces at up, down, left, right plus corners). Final state at 43/144=30% voids.

The number of neighbors can also be adjusted in a 3-D model. The standard cubic stencil would include 6 neighbors associated with the cube faces (left, right, top, bottom, front, back). But possible additional neighbors also exist including 12 at the edge locations and 8 at the corners for a total of 26

Figure 5 shows these three possibilities 6, 18, or 26 neighbors. In addition to these discrete levels one might also imagine the scenarios in which not all neighbors are "created equally." For instance, since it has been observed that nucleation seems to preferentially progress in the [010] direction (i.e. long axis of the rhombus) [8,15] one might imagine a case in which only some pairs of the corners or edges were included instead of all. The algorithm described above is agnostic to the number of neighbors; the only requirement is that it must be symmetric from one block to its neighbor. For instance, if the upper right side edge is included in the stencil, the lower left side edge must be also so that the neighbor can "reach backward" as the original block "reaches forward." So this allows pairs of neighbors to be included; we used as number of neighbors: 6, 8, 10, 12, 14, 16, 18, 20, 22, 24, and 26 in this work. Others have considered more than 6 neighbors; reference [19] gives a critical percolation limit for a 26 neighbor case as ~9.7% in contrast to the 31.17% for the 6 neighbor stencil.

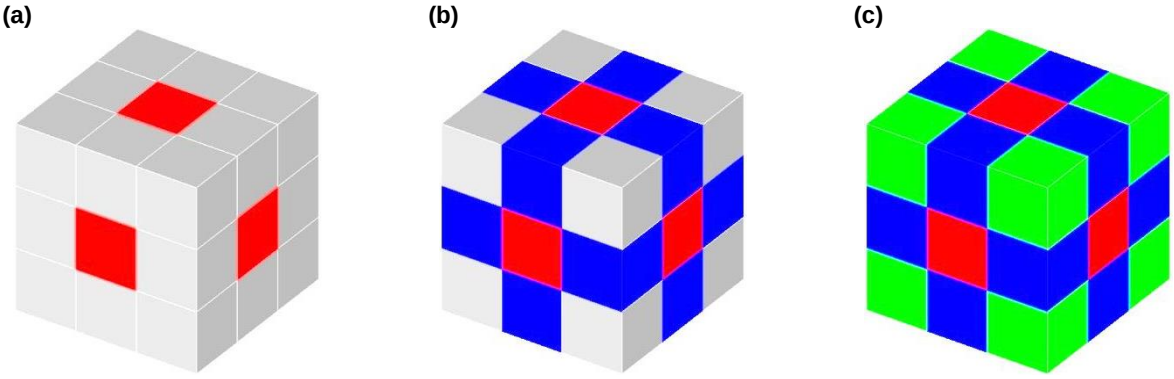

Fig. 5: Possible neighbors surrounding the center cube: (a) 6 neighbors at the cube faces; (b) 6 cube faces + 12 edges = 18 total; (c) 6 cube faces + 12 edges + 8 corners = 26 total.

The Newman-Ziff MC algorithm uses a tree technique to track clusters efficiently. Details are given very clearly in Ref. [18] and a version of their code has been published on the internet, so here we will not describe in detail the methodology used. But as a short description, some of the important concepts are:

- Each site within the domain has an integer "pointer" variable attached. The pointer has three possible values which indicate various states: "empty" = site is in initial state, positive = site is part of a cluster, negative (but non-empty) = root of a cluster.
- Positive values of the pointer refer to the index location of another site in the connected cluster whose pointer, in turn, points to another (recursively) until finally it arrives at site known as the "root" (i.e. twig pointing to small branch pointing to large branch to trunk to root).
- The pointer at the root site of the cluster itself contains a negative number (the negative of the cluster size) so the recursive pointer-checking routine knows when to stop looking.
- Initially each site's pointer is set to a value of "empty" (defined as the negative of the [total number of sites+1]) which indicates that the site is in its initial (i.e. unreacted) state.
- When a site is chosen, if all neighbors are "empty" then the site's pointer is initialized with a value of -1, indicating it is a root site and that the cluster size is 1.
- Otherwise, if there is one non "empty" neighbor to a chosen site, the site is joined to that neighbor's cluster. This is done by setting the site's pointer such that it points to the index number of the neighbor site's root site. The pointer at the root is adjusted to reflect the size of the expanded cluster.
- If a chosen site is neighbor to two or more clusters (say the new site is a bridge between clusters), they will be combined into a single cluster. This is done by finding the largest of the clusters and reassigning the root pointers of all the other clusters to point to the largest cluster's root then adjusting the overall root to reflect the size of the combined cluster.
- In determining connectivity to the outside, we define an extra site which represents the outside and assign the first layer of sites as having that extra ("outside") site as a neighbor. Once interior sites become connected to the outside site, they share a common root and hence connectivity can be easily checked.

Since our overall algorithm induces a changing set of sites available for inclusion (e.g. see the boxes with "+" symbols in Figures 3 and 4 which change as sites become voids), we cannot use the *a priori* randomization method proposed by Newman and Ziff in which each site is assigned an order in which it will be included. Instead we simply choose random numbers associated with the i, j, and k indices associated with the three coordinates of each site within the domain. If the chosen i, j, k coordinates are associated with a site that is not available for reaction (outside the "zone of reaction") we simply skip that set of numbers and choose another (although each time a set of coordinate index numbers is chosen, we do include that attempt in an accumulator variable so we can keep track of the temporal evolution). If the chosen i, j, k is one within the "zone of reaction" it is included and clusters are included using the Newman and Ziff tree structure approach.

RESULTS

Monte Carlo simulations were run to examine the effects of number of neighbors and particle size. Most of the simulations were performed with spherical particles, though rectangular parallelepipeds, cubes, and general ellipsoids were also used. Because this approach is based on sites within a numerical lattice, there is not specifically an associated length scale. Rather, the overall geometry is defined in terms of "pixel" or "voxel" size (i.e. the size of the constituent cubes). In this respect, the geometry is dimensionless.

***Limiting Void Values at Simulation Completion*.**

Figure 6 gives some sample results showing run-to-run variations for 100 MC runs of a sphere of radius 150 pixels. The number of neighbors was varied using values of 6 (faces only), 18 (faces and edges) and 26 (faces, edges, corners) neighbors. The effect was significant. With a 6 neighbor stencil the limiting void fraction was 42.34%; with 18 neighbors the void fraction dropped to 18.73%; with 26 neighbors the limiting value was 13.39%. Standard deviations for each of these sets of runs were less than 0.01%, indicating a remarkable consistency.

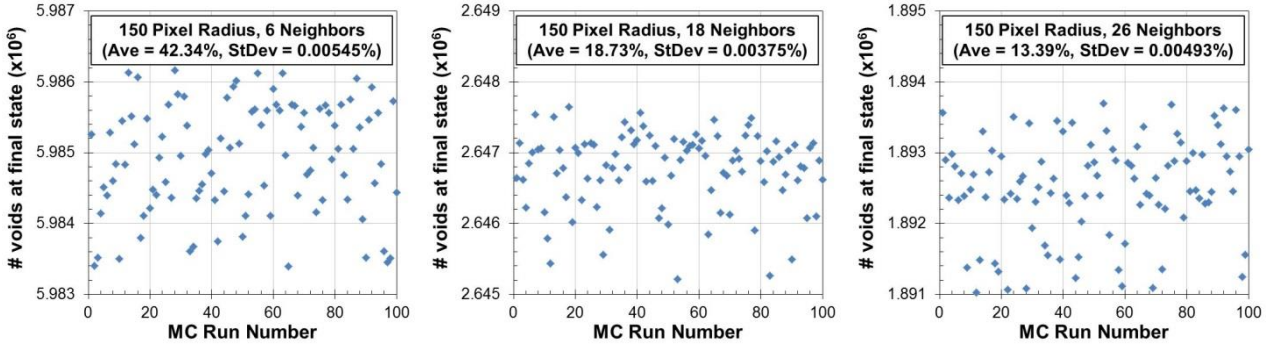

Fig. 6: Total voids at final state for 100 MC runs for a sphere of radius 150 pixels. The sphere had 14,136,576 possible sites [pixels] using: 6 (left graph), 18 (middle), or 26 (right) neighbors. Average void fractions were 42.34%, 18.73% and 13.39% respectively and standard deviations were in the 530 to 770 site ranges (0.00375 to 0.00545%)

Figure 7 shows the effect of the number of neighbors on the limiting void fraction for spheres of various radii. Each of the points represents a series of 100 simulations. The larger sizes show remarkably similar trends, with barely any difference from radii of 150 down to 50 pixels. However, once the sphere radius gets down below about 25 pixels, there begins to be a noticeable difference. At a radius of 5 pixels, the statistics are less well-defined with an appreciable standard deviation occurring. This results from the small number of possible sites (only 552) in the domain where the statistics of large numbers does not apply.

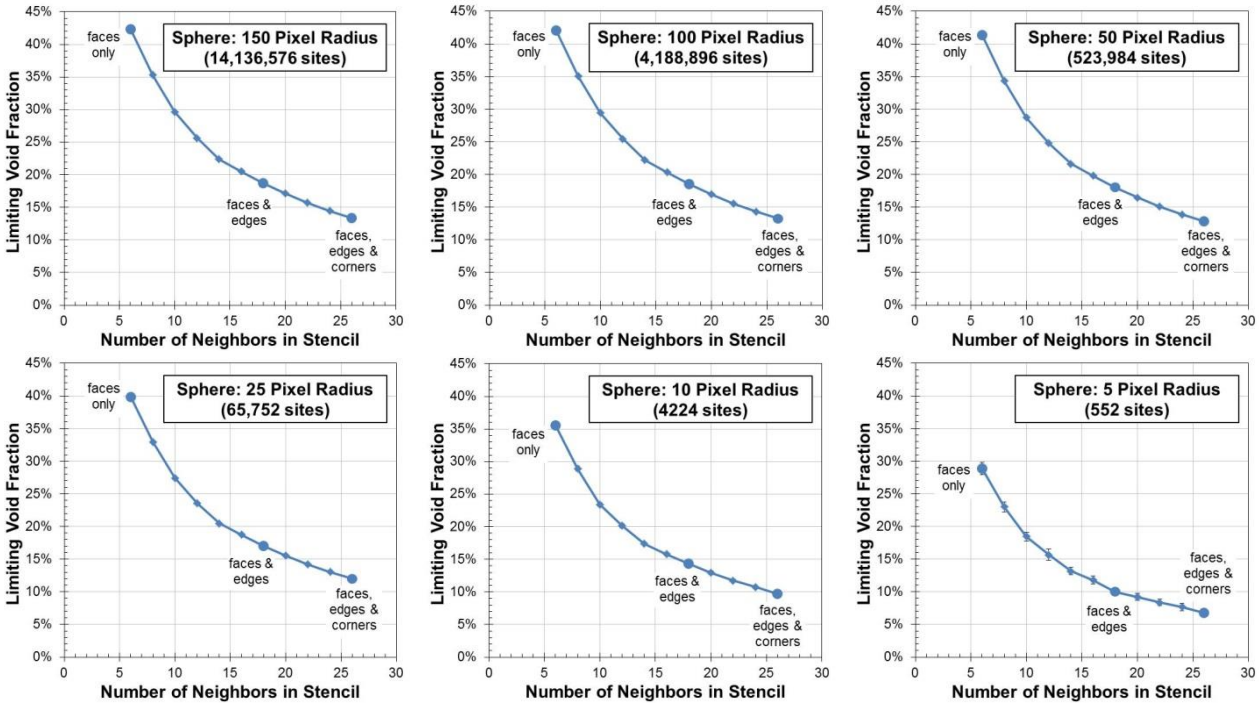

Fig. 7: Limiting void fraction as a function of number of neighbors included in stencil at six different sphere radii: 150, 100, 50, 25, 10, and 5 pixels. These represent the average of 100 runs for each data point. The standard deviation is included here (plotted as error bars) but is smaller than the marker size for each except for the smallest sphere sizes.

Figure 8 (a) shows the overall trend of the MC simulations with respect to particle size and number of neighbors included. Spheres of radii from 2 to 200 pixels were included in this study. At large particle sizes, the limiting void fractions seem to asymptotically approach constant values. At small sizes, the limiting void fraction is heading toward zero. In fact, the algorithm as described above breaks down (no voids can be inserted) below a sphere radii of 3 pixels for all cases except 6 or 8 neighbors.

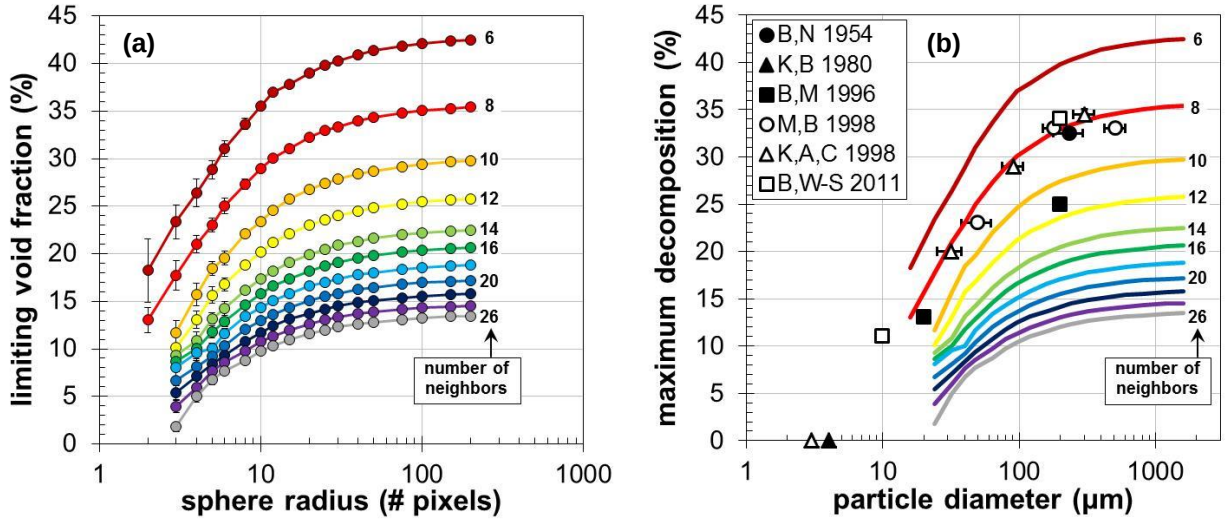

Fig. 8: (a) MC simulation results showing limiting void fraction as a function of sphere radius (non-dimensional in terms of number of pixels). (b) Same MC results as in (a) but abscissa is scaled by assuming that each pixel represents 4 μm in physical length. Also shown is the decomposition level data for AP from Refs. [2-8], previously plotted in Fig. 1.

Figure 8 (b), represents an attempt to relate the dimensionless quantities from the MC simulations with an actual physical dimension. This is done by making the assumption that the pixel length scale is 4 μm. The basis for this length scale are some statements from Khairetdinov and Boldyrev: "characteristic thickness of the walls of this sponge-like structure was 3-5 μm" and "new germs arise mainly in the nearest neighbour (4-6 μm)" [8]. The abscissa of Fig. 8 (b) is also given in terms of particle diameter instead of radius, for a more direct comparison with experimental results. The decomposition limit data as a function of particle size previously presented in Fig. 1 has been superimposed on Fig. 8 (b). For simplicity of comparison, in Fig. 8 (b) the individual data points and error bars from the MC simulations have been removed; only the overall curves are retained. Note the similarity between the trends observed in experiment and the results of the MC simulations. The agreement seems to be best with the MC simulations performed with 8 neighbors (6 cube faces, plus 2 additional edges in one diagonal direction).

***Pseudo Time Dependency*.**

It has been well-established that in most cases (absent special preparation by doping, applying a catalyst, etc., cf. Refs. [1, 8]), the decomposition of AP has a sigmoidal time-dependency with an induction period, followed by an acceleratory period up to a maximum rate, then subsequently decelerating to an asymptotic limit. Figure 9 includes two examples of this behavior from the literature: Ref. [2] because it was a very early observation (left graph) and Ref. [20] because it is a particularly nice data set with results even at very small extents of reaction (right graph including insets).

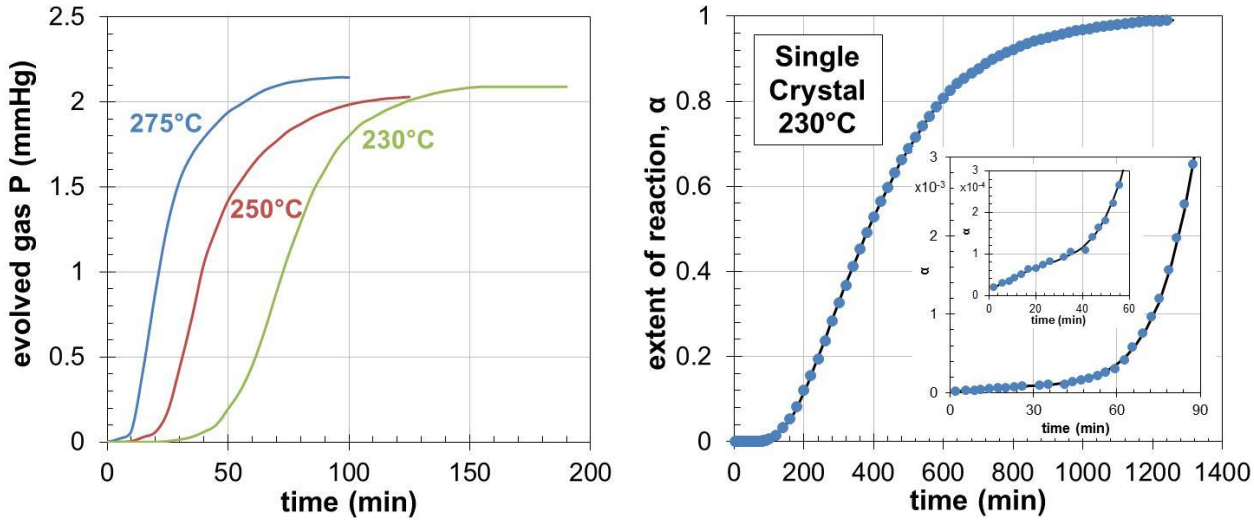

Fig. 9: Examples of AP decomposition data from the literature. Left: polycrystalline AP data adapted from Bircumshaw and Newman [2]; Right: single crystal data adapted from Jacobs and Ng [20].

Strictly speaking, our MC method is not a time-dependent algorithm. However, it can be adapted to give pseudo time-dependent results by making certain assumptions. For instance if we assume that since they are done in series, each attempt (referred to here as an "MC step") to choose a random site for decomposition represents a certain quantity of time. The number of MC steps will be incremented whether the attempt succeeds (i.e. the site decomposes) or fails. This may or may not be accurate in terms of representing reality (for instance, there is nothing to stop multiple sites in a crystal from decomposing simultaneously), but this serves as a first-cut approach at addressing the time-dependency in a simple fashion.

Figure 10 gives examples of the pseudo time-dependent evolution of the void fraction for spherical particles of radius 100 pixels from MC simulations. Shown are the void fraction for pores connected to the outside; a similar fraction for unconnected, blind pores; and the total porosity (sum of the

two parts). Figure 10 (a) and (b) give the result for baseline cases with 6 and 8 neighbors. Note that the both the total voids and the outside-connected voids produce a sigmoidal response complete with induction, acceleration and deceleration, reminiscent of the experimental AP decomposition results. There are reasons to select either "total voids" or "outside-connected voids" as the most appropriate for comparison. The total voids would represent the amount of reaction that has occurred. On the other hand, one might argue that until the voids are connected to the outside, there is no way for the gases to escape and thereby be registered as a measured quantity such as mass loss or gas accumulation.

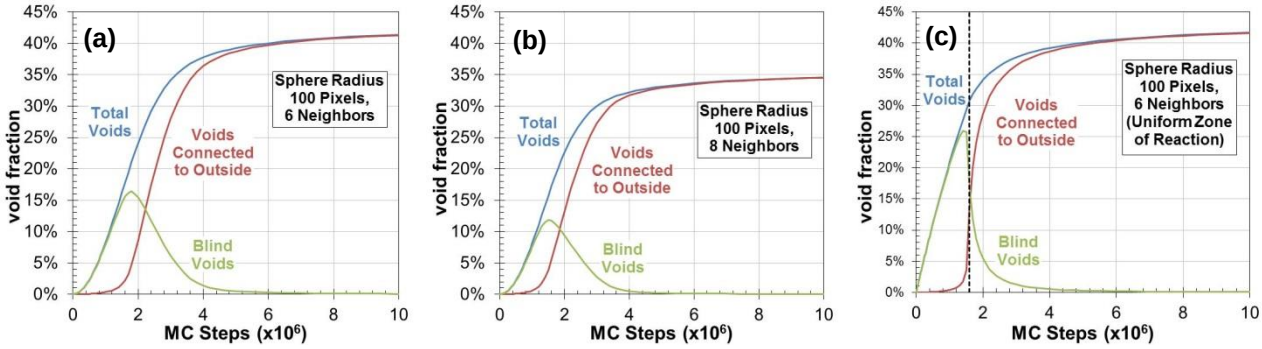

Fig. 10: Pseudo time dependency of MC simulations (time is assumed proportional to number of MC steps taken), showing evolving fractions of total voids, voids that are connected to the outside and unconnected (blind) voids for a sphere of radius 100 pixels. (a) baseline algorithm with 6 neighbors; (b) baseline with 8 neighbors; (c) 6 neighbors with the "zone of reaction" assumed to cover the entire particle from the beginning (dashed line represents point where outside-connected voids suddenly increase, occurring at ~31% void fraction and consistent with traditional percolation theory, cf. Table 1).

Figure 10 (c) shows a 6 neighbor simulation with a slightly modified algorithm. This time, instead of the zone of reaction only initially applied at the layer right below the surface, it is applied everywhere throughout the domain from the beginning. This has the effect of eliminating the "induction time" for the total voids curve, since virtually any site that is chosen (except actually at the surface) will be an acceptable location. So the sigmoidal shape is modified—the highest rate for total void formation is at the very beginning of the simulation. Another interesting observation is that there is a specific point during the simulation in which the outside-connected voids suddenly jump up very precipitously, as indicated by the dashed line in the figure. It turns out that this peak in "connecting" occurs at the point where the total void fraction is right about 31%. In essence, the connected void cluster has reached a percolating state; and this happens right when expected (cf. the critical value given in Table I).

***Structure / Appearance*.**

One of the hoped-for results of this study was that the porous structures observed in microscopic images from AP particle decomposition might be reproduced by the MC simulations. Figure 11 shows some selected images of decomposed AP particles (some single crystals, some composite) at various stages of decomposition. Note that there are various structures present. Some images, namely (b)-(d), show very angular-looking pores (square or rhombus cross section), with many of the pores having a size on the order of 3 μm. Others, such as (e)-(g), also from single crystal experiments, seem to exhibit a significantly different profile. They show a rounder pore cross section, together with long, slender "fingers" near the surface and at late stages, an almost a coral-like overall appearance.

Figure 12 shows some images from two different MC simulations. Part (a) shows a sphere of radius 50 pixels with 6 neighbors (41.3% porosity) and (b) shows an ellipsoid of semi-major, semi-minor axes of 50 x 50 x 100 pixels with 8 neighbors (34.4% porosity). Because of the 3-D nature of the problem, it is difficult to visually verify the connectedness of the porosity in a 2-D image, but every pore in the interior of these particles is, in fact, connected to the outside. The inset of Fig. 11 (b) gives some idea of the structure.

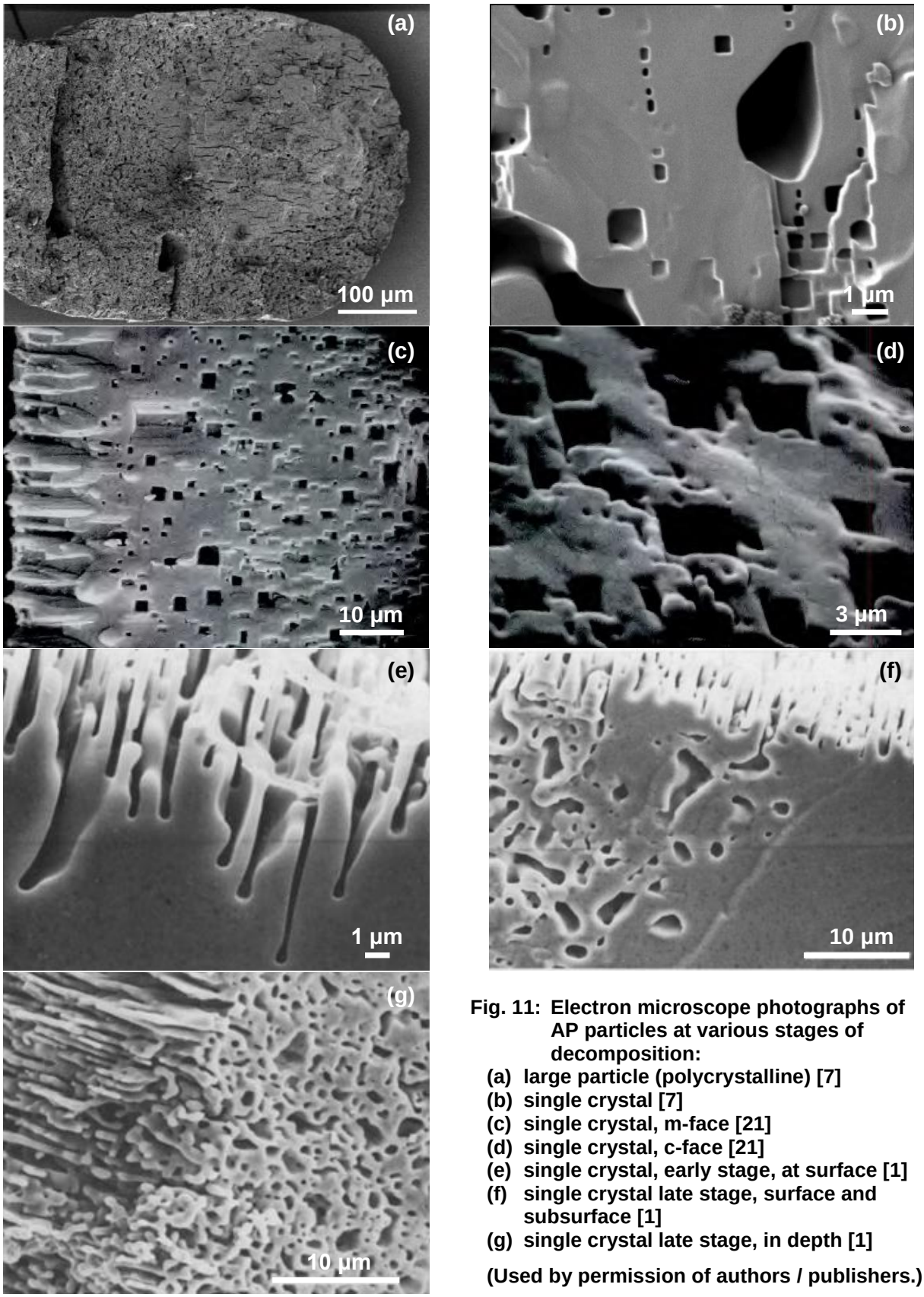

Fig. 11: Electron microscope photographs of AP particles at various stages of decomposition:

- **(a) large particle (polycrystalline) [7]**
- **(b) single crystal [7]**
- **(c) single crystal, m-face [21]**
- **(d) single crystal, c-face [21]**
- **(e) single crystal, early stage, at surface [1]**
- **(f) single crystal late stage, surface and subsurface [1]**
- **(g) single crystal late stage, in depth [1]**

(Used by permission of authors / publishers.)

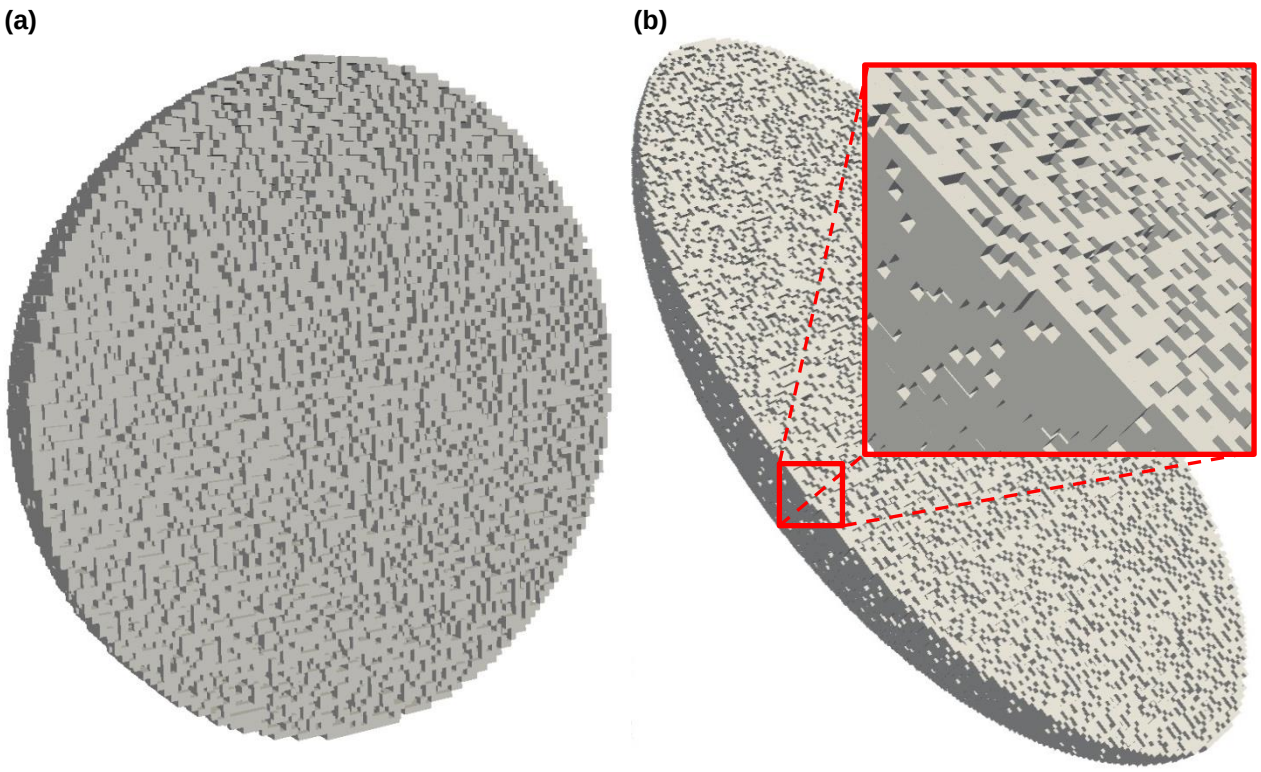

Fig. 12: Cut-away images of final states for two simulations: (a) Sphere of diameter 100 pixels with 6 neighbors in stencil; final porosity is 41.3%. (b) Ellipsoid of size 100x100x200 pixels with 8 neighbors; final porosity is 34.4%. Detail at one edge location is shown.

While there are certainly some areas of agreement in the visual comparisons, other areas are lacking. The square to rhombus cross section from Fig. 11 (c)-(d) seem to be at least qualitatively captured by the MC simulation; the shapes are similar and the 3 μm characteristic pore size seems to match well with the 4 μm pixel size which gave the best fit to the data in Fig. 8 (b). In contrast, the coral-like geometry observed in Ref. [1] as in Fig. 11 (e)-(g) seems to be substantially different, both in terms of pore surface morphology (much rounder) and the pore size, which appear to be generally <1 μm. At this point, a resolution of this discrepancy is still elusive; the authors of both Refs. [1] and [21] had used single crystal AP.

CONCLUSIONS

A Monte Carlo approach has been employed to examine the decomposition of ammonium perchlorate, with the aim of gaining insight into the peculiar decomposition cessation phenomena. Rules were developed for the MC approach which utilized percolation theory and algorithms. Thousands of simulations were performed to investigate the effect of particle size and the number of neighbors in the lattice stencil on the final limits.

Particle size effects were well represented by the algorithm and experimental data could be matched quite reasonably if pixel sizes were assumed to have a physical dimension of 4 μm. This assumption seems at least plausible based on statements from the literature and electron microscope photographs.

Time-dependency effects were estimated by assuming that the MC attempted steps are proportional to elapsed time. This results in a sigmoidal shape for the void fraction as a function of number of steps (pseudo time), which qualitatively agrees with consensus from numerous experiments.

However, quantitative agreement in terms of absolute temporal behavior (including temperature effects on decomposition rates) is not possible with the current algorithm.

The geometrical structure resulting from the MC method was compared with photographs of decomposed AP particles. Qualitative agreement was observed with respect to characteristic pore shapes and connectivity with some of the experimental results, but other photographs from nominally similar tests appeared to be fundamentally different. It is not clear why.

This work has not probed the entire field of ammonium perchlorate decomposition. There are still conflicting ideas and observations which have yet to be resolved. However, it does appear that percolation theory in conjunction with appropriate rules can be used to represent much of the observed phenomena.

ACKNOWLEDGMENTS

This project was supported financially by the Joint Munitions Program (JMP) under Technical Coordination Group-III (TCG-III). The helpful reviews by Jeff Kay and Cole Yarrington are appreciated.

REFERENCES

[1] A. K. Galwey and M. A. Mohamed, "The Low Temperature Thermal Decomposition of Ammonium Perchlorate: Nitryl Perchlorate as the Reaction Intermediate," *Proceedings of the Royal Society of London, A*. 396 (1984) pp. 425-440.

[2] L.L. Bircumshaw and B. H. Newman, "The Thermal Decomposition of Ammonium Perchlorate, I. Introduction, Experimental, Analysis of Gaseous Products, and Thermal Decomposition Experiments," *Proceedings of the Royal Society of London. Series A, Mathematical and Physical Sciences*, Vol. 227, (1954), pp. 115-132.

[3] Minier, L.; Behrens, R., Thermal Decomposition Characteristics of Orthorhombic Ammonium Perchlorate (o-AP)," *17th JANNAF Propulsion Systems Hazards Subcommittee Meeting*, Tucson, AZ, CPIA Publication #681. (1998) Vol. 1, pp. 57-72.

[4] Behrens, R.; Minier, L., "The Thermal Decomposition Behavior of Ammonium Perchlorate and an Ammonium-Perchlorate-Based Composite Propellant," *33rd JANNAF Combustion Meeting*, Monterey, CA, 1996; Vol. CPIA Publication # 653 (2), pp. 1-19.

[5] R. Behrens and D. Wiese-Smith, "Understanding Reactions that Underlie Slow Cookoff Response of Ammonium Perchlorate (AP) and Modified AP," *44th JANNAF Combustion Meeting*, Arlington, VA, CPIA Publication #1849 (2011).

[6] K. J. Kraeutle, A. I. Atwood, and P. O. Curran, "The Partial Decomposition and Sublimation of Propellant Grade Ammonium Perchlorate: Effect of Temperature, Time, and Particle Size," *JANNAF 35th CS, 35th APS, and 17th PSHS Joint Subcommittee Meeting*, Tucson, AZ, CPIA Publication 681 (1998), Vol. 1, pp 45-56.

[7] J. J. Kay, D. Wiese-Smith, A. Highley, and S. Maharrey, "Role of Internal Defects in Promoting Thermal Decomposition of Ammonium Perchlorate," *JANNAF 45th CS, 33rd APS, 33rd EPSS and 27th PSHS Joint Subcommittee Meeting*, Monterey, CA, Dec 3-7, (2012) CPIAC JSC CD-70.

[8] E. F. Khairetdinov and V. V. Boldyrev, "The Mechanism of the Low-Temperature Decomposition of NH_4ClO_4," *Thermochimica Acta*, 41 (1980) pp. 63-86.

[9] A. E. H. Tutton, "The Alkali Perchlorates and a New Principle Concerning the Measurement of Space-lattice Cells," *Proceedings of the Royal Society of London, Series A*, 111 (1926) pp. 462-491.

[10] P. J. Herley, P. W. M. Jacobs, and P. W. Levy, "Dislocations in Ammonium Perchlorate," *Journal of the Chemical Society A: Inorganic, Physical, Theoretical*, (1971) pp. 434-440.

[11] V. V. Boldyrev, "Thermal Decomposition of Ammonium Perchlorate," *Thermochimica Acta* 443 (2006) pp. 1-36.

[12] V. V. Boldyrev, Yu. P. Savintsev and T. V. Moolina, "On the Mechanisms of Formation and Growth of the Nuclei in the Thermal Decomposition of Ammonium Salts," in *Proceedings of the 7th International Symposium on the Reactivity of Solids*, Bristol, 17-21 July 1972, Chapman and Hall, (1972) pp. 421-430.

[13] A. V. Raevskii and G. B. Manelis, “Development of Reaction Centers with Thermal Decomposition of Orthorhombic Ammonium Perchlorate and the Role of Dislocations in this Process,” *Goreniye I Vzryv, Izd vo Nauka*, Moscow, (1972) pp. 748-751 (in Russian); translated as FTD-MT-24-2024-74, Foreign Technology Division, Wright-Patterson AFB, OH, (1974).
[14] K. J. Kraeutle, “Scanning Electron Microscopy of Pure Ammonium Perchlorate After its Reaction in the Orthorhombic and Cubic Phases,” *Proceedings of 7th JANNAF Combustion Meeting* Johns Hopkins University, Applied Physics Laboratory, Howard County, Maryland, 13-15 October 1970, CPIA Publication 204 (1970) Vol. 1, pp. 97-111.
[15] A. V. Raevskii and G. B. Manelis, “Concerning the Problem of the Decomposition of Ammonium Perchlorate” a.k.a. “On the Mechanism of Decomposition of Ammonium Perchlorate,” *Doklady Akademii Nauk SSSR*. 151 (4) (1963) pp. 886-889 (in Russian) translated as: FTD-TT-64-768, Foreign Technology Division, Air Force Systems Command, Wright-Patterson AFB, OH (1964).
[16] A. K. Galwey and M. A. Mohamed, “Nitryl Perchlorate as the Essential Intermediate in the Thermal Decomposition of Ammonium Perchlorate,” *Nature* 311 (1984) pp. 642-645.
[17] A. G. Hunt, “Percolation Theory,” *Percolation Theory for Flow in Porous Media*, Berlin Heidelberg: Springer, (2005) pp. 1-31.
[18] M. E. J. Newman and R. M. Ziff, “Fast Monte Carlo Algorithm for Site or Bond Percolation,” *Physical Review E* 64 (2001) 016706.
[19] M. Rosso, J. F. Gouyet, and B. Sapoval, “Gradient Percolation in Three Dimensions and Relation to Diffusion Fronts,” *Physical Review Letters*, 57 (1986) pp. 3195-3198.
[20] P. W. M. Jacobs and W. L. Ng, “A Study of the Thermal Decomposition of Ammonium Perchlorate Using Computer Modelling,” *Reactivity of Solids*, Proceedings of 7th International Symposium on the Reactivity of Solids, Bristol, England, July 1972, J. S. Anderson, M. W. Roberts, and F. S. Stone, eds., (1972) pp. 398-410.
[21] K. J. Krauetle, unpublished photographs, ca. 1969, provided courtesy of T. Hedman, NAWCWD, China Lake. See also T.L. Boggs and K.J. Kraeutle, “Role of the Scanning Electron Microscope in the Study of Solid Rocket Propellant Combustion, I. Ammonium Perchlorate Decomposition and Deflagration,” *Combustion Science and Technology*, 1 (1969) 75-93.